Sensors & Actuators: B. Chemical 337 (2021) 129795

Contents lists available at ScienceDirect

Sensors and Actuators: B. Chemical

journal homepage: www.elsevier.com/locate/snb

Brain-implantable multifunctional probe for simultaneous detection of glutamate and GABA neurotransmitters

Nicolaie Moldovan [a,*], Iuliu-Ioan Blaga [a], Sanjeev Billa [b], Imran Hossain [b], Chenggong Gong [b], Claire E. Jones [c], Teresa A. Murray [c], Ralu Divan [d], Shabnam Siddiqui [c,e], Prabhu U. Arumugam [b,c]

[a] Alcorix Co., Plainfield, IL, 60544, United States
[b] Institute for Micromanufacturing (IfM), Louisiana Tech University, Ruston, LA, 71272, United States
[c] Center for Biomedical Engineering and Rehabilitation Science (CBERS), Louisiana Tech University, Ruston, LA, 71272, United States
[d] Center for Nanoscale Materials, Argonne National Laboratory, Lemont, IL, 60439, United States
[e] Louisiana State University Shreveport, Department of Chemistry and Physics, Shreveport, LA, 71115, United States

ARTICLE INFO

Keywords:
Amperometry
Ultramicroelectrode
Neurotransmitter
Microfluidic
Glutamate
GABA

ABSTRACT

Glutamate (GLU) and gamma-aminobutyric acid (GABA) are neurotransmitters (NTs) with an essential role in signal transmission in the brain. Brain disorders, such as epilepsy, Alzheimer's and Parkinson's diseases, and traumatic brain injury can be linked to imbalances in the GLU-GABA homeostasis that occurs in sub-second to seconds time frames. Current measurement techniques can detect these two NT concentrations simultaneously only *in vitro*. The present work reports on the fabrication of a silicon multifunctional biosensor microarray probe for sub-second simultaneous GLU-GABA detection in real-time, with excellent analyte sensitivity and selectivity and *in vivo* capabilities. The novel Si probes feature four surface-functionalized platinum ultramicroelectrodes (UMEs) for simultaneous amperometric detection of GLU and GABA with a sentinel, and a built-in microfluidic channel for the introduction of neurochemicals in the proximity of the UMEs. The microchannel also allows functioning of an On-Demand In-situ Calibrator that runs *in-situ* biosensor calibration. The probe exhibited excellent robustness at insertion in agarose-gel brain-tissue-mimicking test, and remarkably high hydrogen peroxide sensitivity (a by-product of GLU-GABA enzyme biosensor) with values on the order of 5000 nA μM^{-1} cm^{-2} and maximum sensitivities of 204 ± 15 nA μM^{-1} cm^{-2} and 37 ± 7 nA μM^{-1} cm^{-2} for GLU and GABA, respectively. Furthermore, the limit of detection of the biosensors reached as low as 7 nM, 165 nM and 750 nM for H_2O_2, GLU and GABA, respectively and a temporal resolution of hundreds of milliseconds during *in vivo* studies using freely moving rats.

1. Introduction

There is an enormous need to further our understanding of the neurobiological mechanisms that underlie aberrant behaviors and disease symptoms related to brain disorders. Often, abnormal neurotransmitter (NT) signaling is an underlying cause of disorders such as epilepsy, Parkinson's and Alzheimer's diseases, traumatic brain injury and drug addiction [1–5]. Two of the major NTs that have a profound role in these disorders are glutamate (GLU), a major excitatory NT, and gamma-aminobutyric acid (GABA), a major inhibitory NT. A proper balance (homeostasis) between GLU and GABA is essential for normal brain function, neuronal activity, information processing and plasticity, and for network synchronization [6–8]. GLU-GABA dysregulation plays a critical role in several psychiatric and neurological disorders, inflammation, and immune cell function and thus, a fundamental understanding of their homeostasis could likely lead to an effective therapeutic strategy for patients with brain disorders [9–12]. However, since GLU and GABA are non-electroactive, it is challenging to detect them in real-time. Currently, the preferred monitoring method is microdialysis [13–17], which allows excellent sensitive chemical resolution but provides poor temporal and spatial resolution (600 s and ~0.1 mm^3, respectively) [18,19]. Since it cannot detect NTs in real-time, it is not suitable to evaluate the role of NT's on behavioral events that occur on the timescale of seconds. As opposed to microdialysis,

* Corresponding author at: 14047 Franklin Ct., Plainfield, IL, 60544, United States.
E-mail address: moldovanl@alcorix.com (N. Moldovan).

https://doi.org/10.1016/j.snb.2021.129795
Received 3 December 2020; Received in revised form 11 March 2021; Accepted 11 March 2021
Available online 15 March 2021

electrochemical biosensors are easy to miniaturize into a microarray and are highly suitable for *in vivo* studies; in the presence of enzymes, they selectively oxidize GLU and GABA into a secondary electroactive product (usually hydrogen peroxide, H_2O_2), which is then detected by amperometry [20–24]. Unfortunately, for GABA detection, this method requires a rather cumbersome process with pre-reactors to exclude interferents and relies on externally applied reagents [25]. Moreover, the conversion of the NT signal to concentrations is inaccurate over time because it merely depends on the calibration carried out *in vitro* and not *in vivo*. Lastly, the relatively large, tapered, shank-shaped microarrays currently in the market are bulky, displace a relatively large volume of tissue, and not suitable for chronic use. This could cause serious problems like glial scar.

Recently, we overcame the problems by demonstrating a biosensor capable of a 26-fold higher sensitivity to GABA, a 4-fold higher sensitivity to GLU, and with no need to add external reagents [26,27]. These results were obtained with commercially available planar platinum (Pt) microelectrode arrays (MEAs) and in-house built Pt microwires bundled into a probe. Additional information on the GLU-GABA biosensing mechanism can be found in the *Supplementary Information* (Fig. S1). The GLU-GABA homeostasis was monitored by simultaneously measuring the H_2O_2 currents generated from the two microbiosensors. Here, we report the design and implementation of a Si microarray probe that operates on a newly conceived principle. It consists of two microbiosensors, one for GLU and one for GABA detection, modified with glutamate oxidase and GABASE enzymes, respectively. By simultaneously measuring and subtracting the H_2O_2 oxidation currents generated from these microbiosensors, GABA and GLU can be detected continuously in real-time *in vitro* and *ex vivo* and without the addition of any externally applied reagents. The detection of GABA by this probe is based upon the *in-situ* generation of α-ketoglutarate from the GLU oxidation that takes place at the GLU microbiosensor. Given the large size of the commercial MEAs and the need of *in vitro* calibration prior to brain implantation, long-term *in vivo* tests were not practical. The goal of the present study is to fabricate and test a multifunctional chronically implantable ultra-small probe with *in-situ* calibration capability that allows high-precision real-time GLU and GABA detection reliably with excellent spatial and temporal resolution *in vivo*. Hereby, we report on developing such a microbiosensor array probe, which integrates into a thin silicon (Si) shaft multiple enzyme-functionalized Pt ultramicroelectrodes, UMEs (25-μm in diameter), and a microfluidic channel for injection of calibration fluid. The probe forms a biocompatible platform for long-term *in vivo* functioning. The four electrodes are designed to detect GLU and GABA simultaneously with a built-in sentinel (control) site. One possible configuration of the four electrodes could be electrode (site) 1 as sentinel, site 2 for GLU, and site 3 and 4 for GABA detection. The GLU site is coated with only glutamate oxidase (GOx). The GABA sites are coated with GOx and GABASE enzymes (details of the sensing mechanism is described in *Fig.S1, Supplementary Information*). In GLU site, GOx facilitated the breakdown of non-electrically active GLU into -ketoglutarate (α-keto), NH_3 and hydrogen peroxide (H_2O_2, Eq. 1). A + 0.7 V bias on the underlying platinum (Pt) microelectrode oxidized H_2O_2 molecules, releasing two electrons per H_2O_2 molecule that induced proportional and measurable current. This current was converted into a GLU concentration based on pre-calibration values. GABA detection is typically facilitated by the application of the GABASE enzyme to an electrode, but an exogenous application of α-keto was previously necessary to facilitate the breakdown of GABA to produce H_2O_2 (Eq. 2). While not a problem for *in vitro* studies, exogenous application of α-keto is unsuitable for *in vivo* studies. However, the product of the GOx reaction with GLU is α-keto (Eq. 3). To create our GABA microbiosensor, we applied both GABASE and GOx to one electrode (site) to record the combined current. We then subtracted the current from an adjacent GOx-coated electrode to derive GABA current [26,27]. The GOx enzyme produced enough α-keto at the GABA-GLU biosensor to support the conversion of GABA to H_2O_2 by GABASE [26,27]. The sentinel is coated identically to the other sites except that no enzymes were used; this provided a means to measure and subtract signals from electrically active interferent molecules, such as ascorbic acid (AA). An additional size-exclusion layer of m-phenylenediamine (mPD), that rejects larger sized molecules, including most AA molecules, was applied over the coated probe sites to mitigate the effect of interferents and further improve selectivity. The present work reports on the fabrication aspects, as well as electrical, microfluidic, and electrochemical tests of the multifunctional probe. Preliminary work on the probe characterization *in vivo* in freely moving rats is described. Our strategies to minimize gliosis are manifold. (1) Our probe design has a pointed tip and electrodes that are further up the shaft, where gliosis in minimal. (2) We avoid damaging blood vessels during implantation. (3) A slow insertion speed is used for implantation. We have implanted much larger devices, including 350-mm diameter gradient index (GRIN) lenses in rodent brain, and had only had a thin layer of glial scarring that did not affect behavior or function. To minimize damage and gliosis, we used a slow 100 μm per minute rate of insertion. We had a very thin glial scar at the end of the lens with sporadic distribution of activated microglia and reactive astrocytes. For the biosensor probes, which have an even smaller profile, we use the same rate of insertion. Detailed *in vivo* evaluation by insertion and operation in live rat brains are ongoing and will be reported elsewhere.

2. Materials and methods

2.1. Design considerations

The tasks for the developed probes were to have multiple GLU and GABA detection sites for reliably measuring concentrations at different positions within the brain and an integrated microfluidic channel for the introduction of chemicals in the immediate vicinity of the UMEs, such as for functioning of an On-Demand In-situ Calibrator (ODIC) that runs *in-situ* sensor calibration for accurate detection. Alternatively, the microchannel can be used to inject specific drugs for testing their NT response. The overall design of the probes had to fulfill incredibly challenging requirements, such as being robust enough to carry out the tissue insertion task, but small enough to not produce significant tissue damage; the electrodes must be large enough for good sensitivity, but small enough for small volume detection; the microchannel must be large enough to allow efficient delivery of chemicals and drugs, but small enough to not be plugged by cells. The general design of the probe fulfilling these requirements is shown in Fig. 1.

2.2. Microfabrication

The fabrication of the Si probe with integrated UMEs and microfluidic channel followed the steps described in Fig. 2. The details of the dimensions of the probe, the UMEs and their spacings and microfluidics are shown in the *Supplementary Information* (Fig. S2). The probes were fabricated on 200-μm-thick, 100-mm-diameter Si (100) prime grade wafers. The thickness of the wafers was chosen to match the thickness of the final probes. Since the thickness of the probe is essential for not inflicting extended brain tissue damage at insertion, 200 μm was a tradeoff between size and robustness of the wafers during processing. About 30 % of the wafers ended up cleaving during various processing steps, but handling experience was gathered and even thinner (*e.g.*, 100 μm) wafers and probes are possible in a future development. For even thinner wafers, there is the possibility to temporarily bond them to carrier wafers, but this exceeded the scope of the first iteration of the probe prototype development phase of this work.

The Si wafers underwent coating with low stress SiN_x (500 nm) by low pressure chemical vapor deposition (LPCVD, Step 1, Fig. 2). 1-μm-wide lines were lithographically patterned and etched into the SiN_x layer by reactive ion etching (RIE), then the etching continued into the Si using deep-RIE (DRIE) -Bosch process, to a depth of ~20 μm to form the

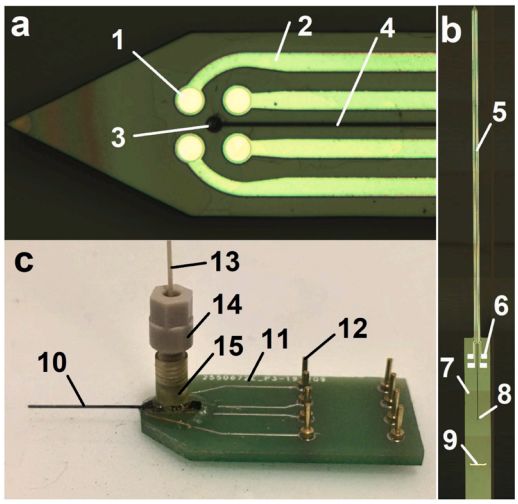

Fig. 1. General design of the brain-implant probe. a) detail of the probe tip; b) Si-probe; c) Final device with Si-probe mounted on a PCB with electrical and microfluidic connectors. 1-Pt microelectrode, 25-μm-diameter (functionalized); 2-SiN_x-insulated Pt leads; 3-Pore opening of microchannel; 4-microchannel sealed with SiN_x; 5-probe shaft of length 1 cm; 6-electrical connection pads for wire-bonding; 7-Si handling chip; 8-inlet pore opening of the microchannel; 9-guide for attaching microfluidic ferrule; 10-Si-probe; 11-custom PCB with Au leads; 12-pin electrical connector; 13-capillary tube; 14-microfluidic connector; 15-microfluidic ferrule glued onto the Si probe after wire bonding. The full dimensional details of the Si-probe can be found in Supplementary data (*Fig. S2*).

ODIC channel (one per device). After removal of the resist, the microchannels were enlarged and acquired a specific cross-section shape during a KOH wet etching (Step 3). The next step (4) was again a LPCVD process for sealing the microchannels, by growing low stress nitride until the edges of the top nitride joined and formed a robust bridge over the channel. A thickness of 2 μm provided good sealing of the channel. Due to the isotropic nature of the LPCVD process, SiN_x was grown also on the inner walls of the channels, but their large cross section assured that the channels had a suitably sized lumen. The inlet and outlet of the channels were patterned with 5-μm-diameter openings at Step 2, so that these are not sealed. Patterning Ti/Pt (5 nm/200 nm, respectively, deposited by electron beam evaporation) electrodes and leads by lift-off followed (Step 5). Ti and not Cr was used as an adhesion layer, to avoid Cr toxicity for implantation into living tissue. The metallization was sealed with plasma-enhanced chemical vapor deposited low stress SiN_x (1-μm-thick). A subsequent lithographic step (7) and RIE opened circular windows atop of the electrodes and contact pads, while also removing the nitride from the microchannel inlet and outlet pores for enlargement (Fig. 3).

The fragility of the probe shafts and wafers, in general, ruled out any type of dicing. A solution was found in delineating the Si-probes entirely by DRIE of Si (Bosch process). Complete etch-through in one step required temporarily attaching the device wafers to carrier wafers using an acetone-soluble wax (Crystalbond 509, Electron Microscopy Sciences, Hatfield, PA) and etching through the back side (Step 8). The details are shown in *Supplementary Information* (Fig. S3). Once etched, the device wafers were carefully detached from the carrier wafers and thoroughly cleaned using 1165 remover, piranha clean and then rinsed with DI water. Finally, the wafers were soaked in acetone and dried by placing them on a 55 °C hot plate, then the temperature was increased to 110 °C, to remove rinse water from the microchannels. Despite the fragility of the probes and wafers, only a small number were damaged

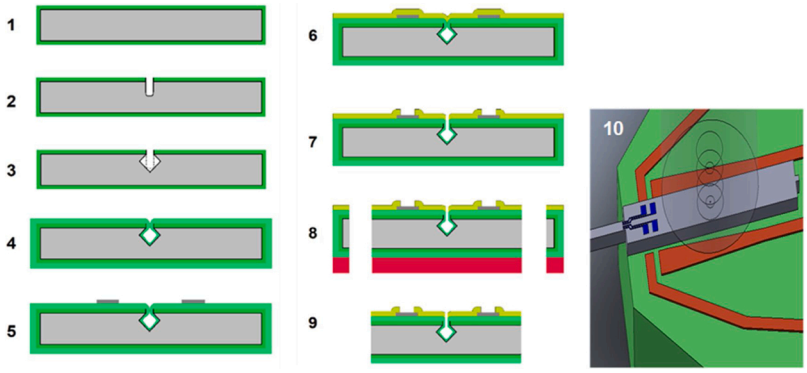

Fig. 2. Fabrication steps: 1-LPCVD SiN_x deposition; 2-lithography with Mask 1, followed by RIE of the SiN_x layer and continued with DRIE of Si; 3-removal of photoresist and enlargement of the microchannel cavity in KOH; 4-Sealing the microchannel with thick LPCVD SiN_x; 5-Patterning of Ti/Pt electrodes and leads by lift off; 6-sealing of leads by SiN_x (PECVD); 7-Lithography and etching of SiN_x in RIE, for exposing the electrodes while leaving the leads covered, as well as opening the inlet and outlet pores of the microchannel, while leaving the channel itself sealed; 8-Lithography with thick photoresist and DRIE of Si to delineate the Si probes; 9-Removal of the thick photoresist and cleaning; (7-9 are sections through the open pore); 10-Mounting of the Si-probe to the PCB with adhesive, followed by wire bonding and mounting the ferules for the microfluidic connectors.

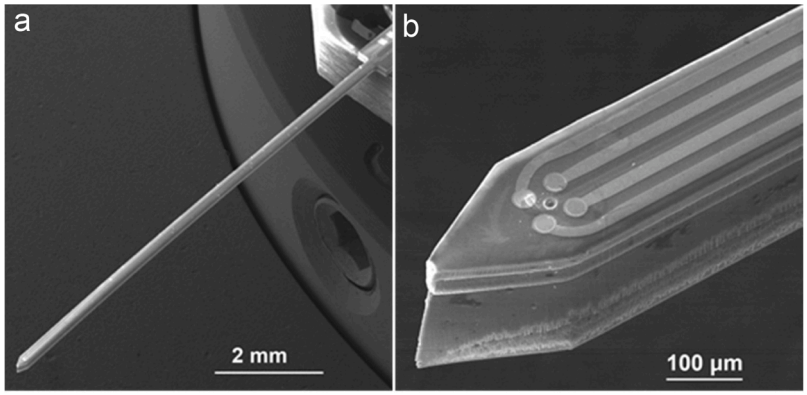

Fig. 3. SEM image of a probe. a) Shaft; b) Details of the tip.

during the multiple steps. Probes were attached to a Si frame through small, easy-to-break Si bridges, which further minimized damage. The details are shown in the *Supplementary Information* (Fig. S4).

Due to the long length of the channels and KOH channel enlargement, accurate alignment with the crystal was done as an initial step to avoid rough steps formation along the channel sidewalls. We followed the strategy proposed by Sato et.al [28] using radial gratings etched into the Si. The alignment position was defined by averaging readings over 16 such radial grating segments present on the wafer. The lithography steps and alignment were performed on a Heidelberg Instruments MLA 150 aligner, which also allowed back-to-front alignment of the final mask for DRIE-through etch. The set of masks contained a series of tests, such as for mask-to-mask alignment, corner-to-corner lithography resolution tests and various resistors for measuring the resistivity and resistance of the metal leads. Once released, the Si probes were mounted onto custom-ordered printed circuit boards (PCBs) with gold metallization. Details of the assembly can be found in *Supplementary Information* (Fig. S5).

2.3. Electrochemical characterization

The microfabricated Pt UMEs were electrochemically cleaned before carrying out any of the electrochemical studies. The cleaning was performed in 0.05 M H_2SO_4 electrolyte solution (Sigma Aldrich) using a potential cycle between −0.3 V to +1.0 V with a 20 mV/s scan rate for 5 cycles in a 2-electrode setup using an Ag/AgCl reference/counter electrode [27,29]. The electrochemical behavior of Pt UMEs was investigated by probing their cyclic voltammetry (CV) response to a 5 mM $K_4Fe(CN)_6$/ 5 mM $K_3Fe(CN)_6$ redox couple in a supporting electrolyte of 1 M KCl. Electrochemical experiments were conducted with an Autolab potentiostat (PGSTAT 302 N, Metrohm USA) in a 3-electrode configuration using the Pt UME as the working electrode, a Pt coil (Alfa Aesar) counter electrode and a saturated calomel reference electrode (SCE, Accumet). All measurements were performed in freshly prepared solutions that were purged with nitrogen for 5 min before use. CV voltammograms were recorded by scanning the potential between −0.3 V and +0.8 V with a scan rate of 100 mV/s. Electrochemical impedance spectroscopy (EIS) spectra were recorded between 100 kHz and 100 mHz with a 10 mV AC signal amplitude (rms value) at open circuit potential (OCP). The impedance data were analyzed by applying a non-linear least square fit to the appropriate theoretical model represented by an equivalent electrical circuit (Fig. 5). All measurements were conducted in 5 mM $K_4Fe(CN)_6$/5 mM $K_3Fe(CN)_6$ in 1 M KCl. For *in vivo* recording, chronoamperometry was done at +0.7 V *vs*. an Ag/AgCl reference/counter electrode implanted next to the silicon probe (2-electrode setup). Out of a total of 30 Si probes assembled (each probe containing four UMEs), 30 UMEs were randomly tested. Five UMEs were found to be unsuitable for further characterization due to poor or no electrochemical signal. The other 25 UMEs were used for the various studies reported herein.

2.4. Chemicals and enzyme coating

Sulfuric acid (CAS. 7664-93-9), potassium chloride (CAS. 7447-40-7), potassium hexacyanoferrate (II) trihydrate (CAS. 14459-95-1), potassium hexacyanoferrate (III) (CAS. 13746-66-2), hydrogen peroxide (CAS. 7722-84-1), L-glutamic acid monosodium hydrate salt (CAS. 142-47-2), gamma-aminobutyric acid (CAS. 56-12-2), bovine serum albumin (CAS. 9048-46-8), glutaraldehyde solution (CAS. 111-30-8,67-56-1), and GABASE (G7509) were purchased from Sigma Aldrich. L-glutamate oxidase (YMS-80049) was purchased from Cosmo Bio USA. Chemicals were used as received.

Briefly, a fresh enzyme matrix solution was prepared that contains bovine serum albumin (BSA, 1%) and the crosslinker, glutaraldehyde (0.125 %), in DI water. We employed the crosslinking method to achieve good stability by retaining enzyme structure and functionality. This solution was mixed with 0.1 U/μL GOx for the GLU microbiosensor and a mixture of 0.1 U/μL GOx and 0.1 U/μL GABASE for the GABA microbiosensor. The prepared aliquots were stored at −80 °C. Prior to GOx enzyme coating, the matrix solution was prepared by mixing 980 μL DI water, 13.3 mg BSA and 6.6 mL glutaraldehyde. Finally, 9 mL of this matrix solution was added to the 0.1 U/μL GOx solution. To prepare the GABA biosensor, a matrix solution was prepared using 970 μL of water in 19.8 mg BSA and 10 mL of glutaraldehyde solution. An 8 mL volume of this matrix solution was added to 0.1 U/μL GOx+0.1 U/μL GABASE. The enzyme solutions containing GOx for GLU microbiosensor and GOx + GABASE for GABA microbiosensor were drop-casted using a micropipettor onto the Pt UMEs (more details in 26, 27). A Nikon stereomicroscope (Model, SMZ18) was employed to dispense one drop (~0.02 μL) of the respective solution manually using a Hamilton syringe (7500 series) on to the electrode sites. The Pt UMEs were modified as GLU microbiosensor using an optimal enzyme concentration of 0.1 U/μL GOx and as GABA microbiosensor using an optimal mixture of 0.1 U/μL GOx and 0.1 U/μL GABASE, respectively. The enzyme coated UMEs were stored in the dark at room temperature for 48 h. Once the enzyme was cross-linked with the enzyme matrix, a size-exclusion layer of mPD was electrochemically coated onto all three coated UMEs. This provides selectivity or specificity to the microbiosensor by preventing the diffusion of the interferents, primarily AA, that are present in high concentrations (up to mM range). A 10 mM mPD solution was prepared in 1 M NaCl and then purged with nitrogen for 30 min before use. The mPD was coated by cycling between +0.2 V and +0.8 V at a scan rate of 50 mV/s for 100 cycles, using a saturated calomel electrode as a reference and counter electrode. After coating, the freshly prepared microbiosensors were stored at 4 °C for 24 h and then calibrated and used.

2.5. Amperometry calibration and detection of NTs

For amperometry calibration, an eight-channel FAST-16mkIII® potentiostat with a 2-electrode configuration, containing an Ag/AgCl reference electrode was used (Quanteon LLC, Kentucky). Amperometry calibrations were conducted at +0.7 V across the Pt UME electrodes in 50 mL 1X phosphate buffered saline solution (PBS) in a glass beaker (details in reference [29]]. The measurements were repeated ($n = 6$ times) and the data was analyzed using FAST analysis® software. Sensitivity toward the analyte (GABA or GLU) was defined as the change in current per unit of analyte addition, which was the slope (pA/μM) of the calibration curves. To calculate the sensitivity per unit electrode area (SS, $nA\mu M^{-1}\ cm^{-2}$), the obtained slope was divided by the Pt UME area ($8.4 \times 10^{-6}\ cm^2$). One-way analysis of variance (ANOVA) was performed to compare differences between conditions. Significance was defined as $p < 0.05$. Error values on plots are shown as mean ± SEM (Standard Error of the Mean).

2.6. Probe implantation and in vivo recording

Male Sprague–Dawley rats were housed on a 12 h light/dark cycle with food and water provided *ad libitum*. All procedures were conducted according to a protocol approved by the Louisiana Tech University Institutional Care and Use Committee and in accordance with the Guide for the Care and Use of Laboratory Animals.

A single probe was implanted into the CA1 region of the hippocampus [27]. Prior to implantation, the shaft, proximal to the connection to the PBP board, was coated with a thin layer of dental acrylic (Ortho-Jet BCA, Lang Dental Manufacturing Company, USA) to prevent breakage of the Si shaft at the PCB board connection. Rats were briefly anesthetized using isoflurane prior to an intramuscular injection of 75 mg ketamine HCl and 0.25 mg dexmedetomidine HCl per 1 kg of animal weight. Using aseptic surgical techniques, a 1.59-mm diameter craniotomy was made 4.6 mm posterior to Bregma, 3 mm lateral to the midline over the right hemisphere. Three 1.25-mm stainless-steel anchor screws (Stoelting Co.) were implanted bilaterally along the outer edge of

the scalp incision as anchors for the implant. The PCB board of the probe was attached to a bulldog clamp on a stereotaxic frame and slowly lowered at 100-μm per min to a depth of 2.5 mm below the pial surface. The probe and screws were encased with dental acrylic to secure the probe to the skull. A topical powder (Neo-Predef, Zoetis) was applied for analgesic, antibiotic, and anti-inflammatory purposes. To bring the rat out of the surgical plane of anesthesia, an intramuscular injection of 1 mg/kg Atipamezole hydrochloride was administered. Rats were monitored until sternal recumbency as regained. Rats were housed individually after surgery.

Prior to recording, each rat was briefly anesthetized in a chamber using 5% isoflurane before attaching the probe to the recording system. For recording, a rat was placed in a standard, clear plastic housing cage without a cover and with corn cob bedding, a bottle of water and chow. A + 0.7 V bias voltage was applied to the microwire biosensors to facilitate oxidation of H_2O_2. The FAST system acquired current data at 1000 Hz which were stored as csv files for offline analysis.

3. Results and discussions

3.1. Microscopy and mechanical characterization

Figs. S3 and S4 (refer to *Supplementary Information*) shows the scanning electron microscopy image of the microchannel details during etching and sealing and a photo of a finished wafer with probes, respectively. The probes were characterized through optical and electron microscopy (Figs. S3 and 3, respectively). Mechanical tests were performed to check the robustness and damage-free insertion into a calibrated agarose gel, of the consistency (*i.e.*, 0.6 % concentration) and above the consistency (up to 1.5 % concentration) of brain tissue, [30] (Figs. S6, S7 and movies 1–3 *of Supplementary Information*). The tests showed that the microfabricated probes are fit for standard insertion procedures [31]. Electrical tests consisted of resistance and leakage resistance measurements of the Pt UMEs, rendering values common for normal practice (details in *Supplementary Information*). Testing the microfluidic integrity and microchannel fluid transport capability was accomplished by pumping air, deionized water, acetone, and a fluorescent dye solution with a syringe micropump through the probes, while observing air bubbles, droplets, or fluorescence at the probe tip in various media. Out of 24 probes tested, 21 showed unobstructed channels, while the three with obstructions originated from a wafer with known smaller lumens. For preserving the cleanliness of the probes in non-destructive quality control testing, acetone was adopted for use, with drying the probes after the test in a vacuum oven at 50 °C for one hour. The characterization and mechanical tests showed a robust manufacturability of probes with full control of their parameters and features.

3.2. Electrochemical characterization

3.2.1. CV analysis

Cyclic voltammograms show sigmoidal curves (Fig. 4), suggesting the dominance of radial diffusion. Such UMEs are preferred for ultrasensitive and low limit of detection biosensing because of their high faradaic (*i.e.* signal) current-to-charging current (*i.e.* noise) ratio (SNR). Here, we observed high SNR values in the order of 115 and above. Another important electrochemical behavior for biosensing is the electrode kinetics. The current gold-standard microelectrode materials for amperometric biosensing are the noble metals, which exhibit fast electron-transfer kinetics and adequate sensitivity [32,33]. Facile kinetics allows the user to avoid large overpotentials for H_2O_2 oxidation in delicate microenvironments like the brain. For UMEs, Tomeš criterion of reversibility [34] of $|E_{3/4}–E_{1/4}| = (60.2\ mV/\alpha\eta)$ is used to describe the electrode kinetics. The $E_{3/4}$ and $E_{1/4}$ are the potentials where $I = 3I_{ss}/4$ and $I = I_{ss}/4$, respectively, I_{ss} being the steady state limiting diffusion current for UMEs, α is transfer coefficient and η is the number of

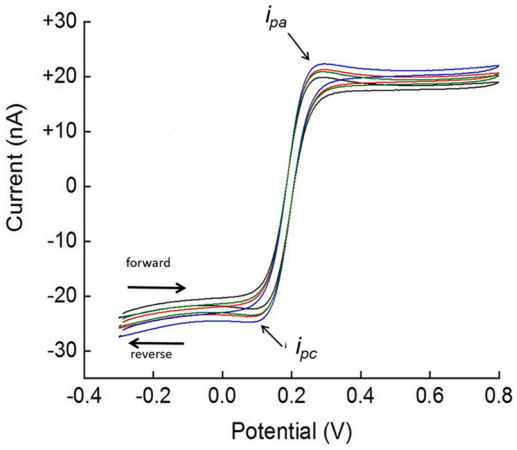

Fig. 4. Overlay of cyclic voltammograms recorded from the four working UMEs within a Si probe. The voltammograms of the four UMEs 1 to 4 are shown in black, red, blue, and green curves. The anodic (i_{pa}) and the cathodic peak (i_{pc}) are noted (forward and reverse arrows). The electrolyte is a 5 mM $Fe(CN)_6^{3-/4-}$ in 1 M KCl solution. Scan rate is 100 mV/s.

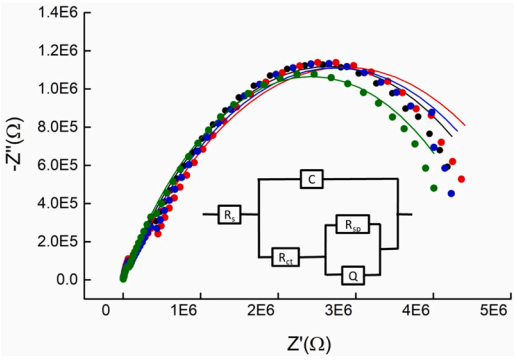

Fig. 5. Representative Nyquist plots of Pt UMEs. EIS spectra of UMEs 1 to 4 were shown as black, red, blue, and green dotted curves, respectively. The solid curves were fitted to the experimental data. The electrolyte is 5 mM Fe $(CN)_6^{3-/4-}$ in 1 M KCl. 10 mV amplitude, 0.1 Hz - 100 kHz. Note. The visual aspect of the curves was not circular but elliptical, due to the difference in the scales of the axes.

electrons involved in the redox reaction. The typical $|E_{3/4}–E_{1/4}|$ value for the UMEs is 27.5 ± 1.44 mV which is very close to the Tomeš potential difference and thus, demonstrates fast kinetics, as expected from an electrochemically cleaned Pt surface. This is because the Pt grain boundaries are etched, and the charge transfer resistance of the Pt grains is significantly reduced with a corresponding increase in the kinetic rate constants during such cleaning process (details in reference [29]). The $|E_{3/4}–E_{1/4}|$ value did not significantly vary among UMEs (ANOVA one-way test, $p < 0.05$). Overlapping cyclic voltammograms with similar amplitudes of the limiting current (~20.4 ± 0.95 nA, n = 6) from these UMEs show the reproducibility in the microfabrication of the probe with comparable UMEs.

3.2.2. Electrochemical impedance spectroscopy (EIS) analysis

The shape of the impedance spectra (Nyquist plots) of UMEs consists of large arcs [35] (Fig. 5). The general behavior of the spectra is very reproducible among the UMEs within a probe and between probes (n = 8, from 4 different probes). The fitted circuit $[R_s(C[R_{ct}(R_{sp}Q)])]$, is similar to the one used for fitting impedance data to a polymer-coated metal surface [36–39]. The five elements of this fitted circuit are solution resistance (R_s), capacitance (C), charge transfer resistance (R_{ct}), constant phase element (CPE) (Q), solution resistance due to Pt grain

boundary (GB) and surface pore defects (R_{sp}). The circuit element values extracted by fitting the experimental data are given in Table 1. R_s models the electrolyte resistance and does not vary much among UMEs. The capacitance C in the circuit models the capacitance of the double layer surrounding the Pt grains of the electrode. The constant phase element Q is introduced to model the time constant dispersion (*i.e.*, variation along the electrode surface of reactivity or of current and potential) and can be linked to Pt GB chemical, microstructural and morphological heterogeneities. The charge transfer resistance R_{ct} is due to grains. In the literature, several models have been developed to describe a pore [40], including N -a parameter ($0 \leq N \leq 1$) for Q that models the behavior of heterogeneous surfaces such as GB. The case $N = 1$ describes an ideal capacitor while the case $N = 0$ describes a pure resistor. The case $N = 0.5$ implies a surface that corresponds to a pore. In Table 1, the extracted values for N are approximately 0.52 showing that the GB and the microstructural defects at or near the GB collectively behave like a pore, *i.e.*, the surface is heterogenous and rough, causing an increase in the impedance. The other circuit element of the pore is the solution resistance within the pores (hence called R_{sp}, where "p" stands for pore). Generally, GB effects are revealed in the fitted models at smaller electrode dimensions, such as our UMEs, when the average grain size is a significantly large fraction of the electrode dimension. Similar observations were reported for other electrode materials [35]. Altogether, the Pt UMEs reported here showed a highly active electrochemical surface that exhibited remarkably high sensitivity towards H_2O_2 (details in the next section).

3.2.3. H_2O_2 calibration

The Pt UMEs were CV cleaned to increase their H_2O_2 sensitivity and improve their biosensor performance [29]. Sensitivity is one of the key metrics for measuring analytes at physiological concentrations, *i.e.*, in the nM to μM range. The Pt UMEs were then calibrated to measure their sensitivity towards H_2O_2, which is the electroactive by-product of the GLU and GABA enzyme-mediated reactions. Sensitivity values in the order of 5000 nA μM^{-1} cm^{-2} were recorded from the UMEs, which are very high compared to the ones reported in the literature (Fig. S8, *Supplementary Information*) and could be due to an increase in the availability of electrocatalytic sites, as reported in [29].

3.2.4. GLU and GABA detection in vitro and in vivo

The calibration was performed after the enzymes were completely crosslinked during the 48-h storage in dark and at room temperature. The calibration curves and the sensitivity values for a linear GLU and GABA range from 1 μM to 40 μM are shown in Figs. 6,7 , respectively. The measured GLU and GABA sensitivity values were in the range of 187 ± 8–204 ± 15 nA μM^{-1} cm^{-2} and 29 ± 3–37 ± 7 nA μM^{-1} cm^{-2}, respectively. These values are comparable to others in the literature and thus, are suitable for cell, tissue, and animal model studies [26,27,29,41,42]. Selectivity is further improved through subtraction of the interferent signal from the "sentinel" site. The sentinel was prepared the same way as the GABA and GLU sites, including mPD coating, except that the matrix coating on the sentinel contained only BSA and glutaraldehyde (*i.e.*, it did not include an enzyme). BSA is an inactive protein of a size that is like GABASE and GOx; this maintains approximately the same rate of diffusion [27]. Similar diffusion rates of interferent molecules at all

Table 1
Values of interfacial parameters of Pt UMEs obtained by fitting [R_s(C[R_{ct}($R_{sp}Q$)])] circuit to experimental data. The % errors for R_s, C, R_{ct}, R_{sp}, Q and N are 7-10 %, 3-4%, 15-17 %, 4-8%, 5-10 % and 2-4%, respectively.

UME #	R_s [KΩ]	C [pF]	R_{ct} [KΩ]	R_{sp} [MΩ]	Q [nmho s^n]	N
1	3.7	273	52.7	5.2	73.1	0.51
2	3.8	286	82.5	5.4	75.6	0.52
3	3.7	306	121	5.5	77.3	0.52
4	3.3	353	44.1	4.8	71.0	0.52

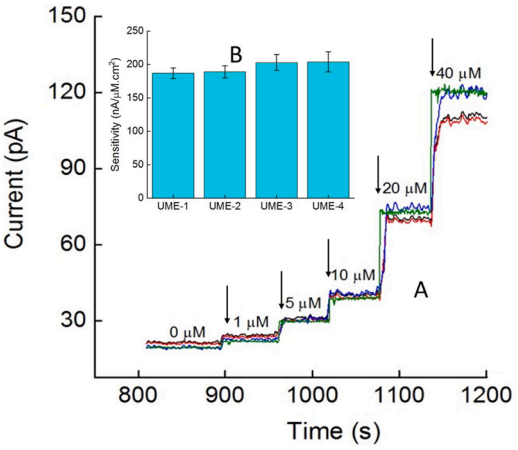

Fig. 6. Characterization of GLU microbiosensors. Measurements were acquired in 1X PBS with a 200-rpm stirring rate at 37 °C. Amperometry parameters were +0.7 V *vs* Ag/AgCl. (A) Representative plot of the response to GLU (stepwise additions of 1, 4, 6, 10 and 20 μM, downward arrows) at the glutamate oxidase (GOx) modified Pt UMEs 1 to 4 which were shown in black, red, blue, and green, respectively. As expected, corresponding stepwise increases in current occurred with increasing GLU concentration. The UMEs were coated with 0.1 U/μL of GOx. (B) shows the GLU sensitivity at each microbiosensor. The sensitivity values of microbiosensors 1 to 4 were 187 ± 8, 189 ± 9, 203 ± 12 and 204 ± 15 nA μM^{-1} cm^{-2}, respectively. Values were shown in mean ± SEM. The sensitivity values among the biosensors were not significantly different (one-way ANOVA, $p < 0.05$).

three biosensors enables subtraction of sentinel current from GABA and GLU current to minimize the effect of interferents. Selectivity is calculated as the sensitivity ratio of GLU or GABA to AA. AA had no effect on current, as seen in *Fig. S9, Supplementary Information*. The average selectivity of the biosensors towards AA is greater than 96 ± 3 (*Fig. S9, Supplementary Information*), which compares well with the literature and is sufficient for *in vivo* studies. The limit of detection (LOD) of the biosensors reached as low as 7 nM, 165 nM and 750 nM for $H2O_2$, GLU and GABA, respectively (*Table S1, Supporting Information*). Currently, we are optimizing the process variables to achieve further improvements in sensitivity values. The initial data from *in vivo* studies using freely moving rats exhibited both sub-second resolution (in 100 ms range) and reliable neurochemical measurements (***Fig. S10***, *Supplementary Information*). The details of the studies will be published in future publications.

4. Conclusions

Novel brain-implantable silicon probes were designed and manufactured for simultaneous detection of GLU and GABA. The probes contain four 25-μm-diameter Pt UMEs that can be surface-modified to detect a wide range of NTs and one microfluidic channel for *in situ* on demand calibration or, alternatively, drug injections, to study NT response to stimuli. The probe's function was tested based on electrochemical detection of H_2O_2 as generated by the reaction of NTs at the specific enzyme-functionalized electrodes, GOx and GOx + GABASE, for GLU and GABA detection, respectively. The probes were tested mechanically at insertion in calibrated brain tissue-mimicking gels, and electrically and amperometrically *in vitro*, showing suitability for *in vivo* studies. The Pt UME recorded highest order of H_2O_2-detection sensitivities of 5000 nA μM^{-1} cm^{-2}. These Pt UMEs when modified with 0.1 U/μL GOx exhibited a maximum sensitivity of 204 ± 15 nA μM^{-1} cm^{-2} for GLU detection and when modified with 0.1 U/μL GOx and 0.1 U/μL GABASE recorded a sensitivity of 37 ± 7 nA μM^{-1} cm^{-2} for GABA detection and a selectivity of 96 ± 3 towards ascorbic acid. The preliminary *in vivo* studies with freely moving rats demonstrated low LOD (in 100's of nM range) with excellent temporal resolution (100 ms

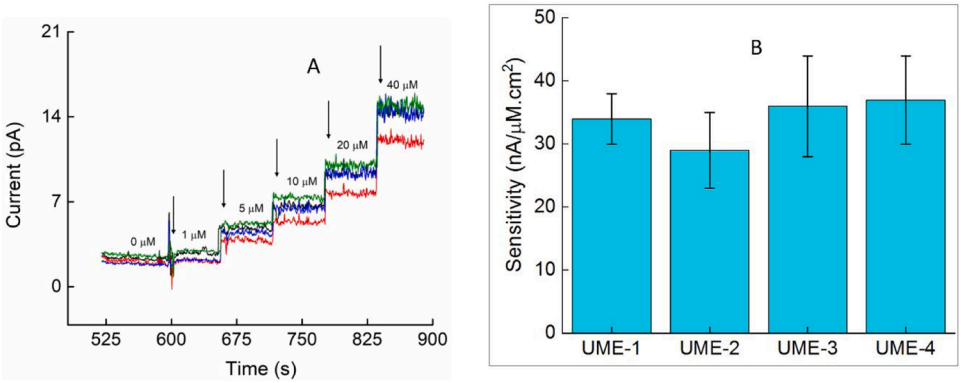

Fig. 7. Characterization of GABA microbiosensors. Measurements were acquired in 1X PBS containing 1 mM α-keto with a 200-rpm stirring rate at 37 °C. Amperometry parameters were +0.7 V *vs* Ag/AgCl. (A) Representative plot of the response to GABA (stepwise additions of 1, 4, 6, 10 and 20 μM, downward arrows) at the GOx/GABA modified Pt UMEs 1 to 4 were shown in black, red, blue, and green, respectively. As expected, corresponding stepwise increases in current occurred with increasing GABA concentration. The UMEs were coated with 0.1 U/μL each of GOx and GABASE. (B) shows the GABA sensitivity at each microbiosensor. The sensitivity values of microbiosensors 1 to 4 were 34 ± 4, 29 ± 3, 36 ± 4 and 37 ± 7 nA μM^{-1} cm^{-2}, respectively. Values are shown in mean ± SEM. The sensitivity values among the biosensors were not significantly different (one-way ANOVA, $p < 0.05$).

range) and reliable neurochemical current measurements. Currently, the multifunctional silicon probes are used to study GLU-GABA dynamics in longitudinal studies (up to a week) involving rat models.

CRediT authorship contribution statement

Nicolaie Moldovan: Probe design and nanofabrication. **Iuliu-Ioan Blaga:** Probes assembly and mechanical testing. **Ralu Divan:** Nanofabrication process development. **Sanjeev Billa**: Probe coating and characterization, Writing – original draft. **Imran Hossain**: Data analysis, Writing – original draft. **Chenggong Gong**: Probe coating protocol development. **Claire E. Jones**: Animal surgery and experiments. **Teresa A. Murray**: Animal experiments, Writing – review & editing. **Shabnam Siddiqui**: Experimental design, EIS analysis. **Prabhu U. Arumugam**: Conceptualization, Writing - original draft, Writing - review & editing, Supervision.

Declaration of Competing Interest

N. Moldovan and I. Blaga are involved with Alcorix Co. in developing for commercialization probes described within the paper, *via* a NIH STTR Phase I project, in which the university partner is the LA Tech group of authors.

Acknowledgments

Research reported in this publication was supported by the National Institute of Neurological Disorders and Stroke (NINDS) of the National Institutes of Health (NIH) under Award Number R41NS115282. The content is solely the responsibility of the authors and does not necessarily represent the official views of the NIH. This work utilized Northwestern University Micro/Nano Fabrication Facility (NUFAB), which is partially supported by Soft and Hybrid Nanotechnology Experimental (SHyNE) Resource (NSF ECCS-1542205), the Materials Research Science and Engineering Center (DMR-1720139), the State of Illinois, and Northwestern University. The authors also acknowledge the use of the Center for Nanoscale Materials, an Office of Science user facility, supported by the U.S. Department of Energy, Office of Science, Office of Basic Energy Sciences, under Contract No. DE-AC02-06CH11357.

Appendix A. Supplementary data

Supplementary material related to this article can be found, in the online version, at doi:https://doi.org/10.1016/j.snb.2021.129795.

References

[1] D.L. Robinson, A. Hermans, A.T. Seipel, R.M. Wightman, Monitoring rapid chemical communication in the brain, Chem. Rev. 108 (2008) 2554–2584, https://doi.org/10.1021/cr068081q.
[2] D.L. Robinson, R.M. Wightman, Rapid dopamine release in freely moving rats, in: A.C. Michael, L.M. Borland (Eds.), Electrochemical Methods for Neuroscience, CRC Press, Boca Raton, 2007, pp. 17–34. https://www.ncbi.nlm.nih.gov/books/NBK2575/.
[3] S.G. Sandberg, P.A. Garris, Neurochemistry of addiction: monitoring essential neurotransmitters of addiction, in: C.M. Kuhn, G.F. Koob (Eds.), Advances in the Neuroscience of Addiction, CRC Press, Boca Raton, FL, 2010, pp. 101–136. https://www.ncbi.nlm.nih.gov/books/NBK53365/.
[4] I. Willuhn, M.J. Wanat, J.J. Clark, P.E. Phillips, Dopamine signaling in the nucleus accumbens of animals self-administering drugs of abuse, Curr. Top. Behav. Neurosci. 3 (2010) 29–71, https://doi.org/10.1007/7854-2009-27.
[5] P.S. Cahill, Q.D. Walker, J.M. Finnegan, G.E. Mickelson, E.R. Travis, R. M. Wightman, Microelectrodes for the measurement of catecholamines in biological systems, Anal. Chem. 68 (1996) 3180–3186, https://doi.org/10.1021/ac960347d.
[6] R. Bhata, R. Axtella, A. Mitrab, M. Miranda, C. Lock, R.W. Tsien, L. Steinman, Inhibitory role for GABA in autoimmune inflammation, PNAS 107 (6) (2010) 2580–2585, https://doi.org/10.1073/pnas.0915139107.
[7] W.L. Caudill, G.P. Houck, R.M. Wightman, Determination of γ-aminobutyric acid by liquid chromatography with electrochemical detection, J. Chromatogr. B Biomed. Sci. Appl. 227 (1982) 331–339, https://doi.org/10.1016/s0378-4347(00)80387-4.
[8] S. Smith, Measurement of GABA in rat brain microdialysates using o-phthaldialdehyde—sulphite derivatization and high-performance liquid chromatography with electrochemical detection, J. Chromatogr. B Biomed. Sci. Appl. 652 (1994) 228–233, https://doi.org/10.1016/0378-4347(93)E0391-3.
[9] C.G. Wong, T. Bottiglieri, O.C. Snead, GABA, gamma-hydroxybutyric acid, and neurological disease, Ann. Neurol. 54 (2003) S3–S12, https://doi.org/10.1002/ana.10696.
[10] R. Bhat, R. Axtell, A. Mitra, M. Miranda, C. Lock, R.W. Tsien, L. Steinman, Inhibitory role for GABA in autoimmune inflammation, PNAS 107 (6) (2010) 2580–2585, https://doi.org/10.1073/pnas.0915139107.
[11] M. Auteri, M.G. Zizzo, R. Serio, The GABAergic system and the gastrointestinal physiopathology, Curr. Pharm. Des. 21 (34) (2015) 4996–5016, https://doi.org/10.2174/1381612821666150914121518.
[12] J. Tian, Y. Lu, H. Zhang, C.H. Chau, H.N. Dang, D.L. Kaufman, GABA inhibits T cell autoimmunity and the development of inflammatory responses in a mouse type 1 diabetes model, J. Immunol. 173 (2004) 5298–5304, https://doi.org/10.4049/jimmunol.173.8.5298.
[13] U.U. Kehr, Fast HPLC estimation of γ-aminobutyric acid in microdialysis perfusates: effect of nipecotic and 3-mercaptopropionic acids, J. Neurochem. 51 (1988) 1308–1310, https://doi.org/10.1111/j.1471-4159.1988.tb03101.x.
[14] H.L. Rowley, K.F. Martin, C.A. Marsden, Determination of in vivo amino acid neurotransmitters by high-performance liquid chromatography with o-phthalaldehyde-sulphite derivatisation, J. Neurosci. Methods 57 (1995) 93–99, https://doi.org/10.1016/0165-0270(94)00132-Z.
[15] A. Andrea, J.F. Monge-Acuna, A high performance liquid chromatography method with electrochemical detection of gamma-aminobutyric acid, glutamate and glutamine in rat brain homogenates, J. Neurosci. Methods 183 (2009) 176–181, https://doi.org/10.1016/j.jneumeth.2009.06.042.
[16] N.J. Reinhoud, Analysis of glutamate, GABA, noradrenaline, dopamine, serotonin, and metabolites using microbore UHPLC with electrochemical detection, ACS Chem. Neurosci. 4 (2013) 888–894, https://doi.org/10.1021/cn400044s.
[17] B. Baily, Thermo-Scientific, 2017 (online), https://tools.thermofisher.com/content/sfs/posters/85830-POPittcon-Neuroactive-09Mar2010-LPN2423-01.pdf.

[18] C.J. Watson, B.J. Venton, R.T. Kennedy, In vivo measurements of neurotransmitters by microdialysis sampling, Anal. Chem. (2006) 1391–1399, https://doi.org/10.1021/ac0693722. March 1.
[19] O.S. Mabrouk, J.L. Han, J.-M.T. Wong, H. Akil, R.T. Kennedy, S.B. Flagel, The in vivo neurochemical profile of selectively bred high-responder and low-responder rats reveals baseline, cocaine-evoked, and novelty-evoked differences in monoaminergic systems, ACS Chem. Neurosci. 2018 (9) (2018) 715–724, https://doi.org/10.1021/acschemneuro.7b00294.
[20] K.N. Hascup, E.C. Rutherford, J.E. Quintero, B.K. Day, J. Burmeister, G. A. Gerhardt, Second-by-second measures of glutamate and other neurotransmitters using enzyme-based microelectrode arrays, in: A.C. Michael, L.M. Borland (Eds.), Electrochemical Methods for Neuroscience, CRC Press, Boca Raton, 2007, pp. 407–450. https://www.ncbi.nlm.nih.gov/books/NBK2567/.
[21] M.G. Garguilo, A.C. Michael, Quantification of choline in the extracellular fluid of brain tissue with amperometric micro sensors, Anal. Chem. 66 (1994) 2621–2629, https://doi.org/10.1021/ac00089a006.
[22] F. Mazzei, Peroxidase based amperometric biosensors for the determination of γ-aminobutyric acid, Anal. Chim. Acta 328 (1996) 41–46, https://doi.org/10.1016/0003-2670(96)00089-X, 1996.
[23] N. Sekioka, D. Kato, R. Kurita, S. Niwa, O. Hirono, Improved detection limit for an electrochemical γ-aminobutyric acid sensor based on stable NADPH detection using an electron cyclotron resonance sputtered carbon film electrode, Sens. Actuators B Chem. 129 (2008) 442–449, https://doi.org/10.1016/j.snb.2007.08.040.
[24] O. Niwa, R. Kurita, T. Horiuchi, K. Torimitsu, Small-volume on-line sensor for continuous measurement of γ-aminobutyric acid, Anal. Chem. 70 (1998) 89–93, https://doi.org/10.1021/ac970740z.
[25] Antec Scientific, ALEXYS Neurotransmitter Analyzer, GABA and Glutamate, Antec Scientific, Application note 213_020#01 (online), 2013.
[26] I. Hossain, C. Tan, P.T. Doughty, G. Dutta, T.A. Murray, S. Siddiqui, L. Iasemidis, P. U. Arumugam, A novel microbiosensor microarray for continuous ex vivo monitoring of gamma-aminobutyric acid in real-time, Front. Neurosci. 12 (2018), https://doi.org/10.3389/fnins.2018.00500. PAGE 500, URL: https://www.frontiersin.org/article/10.3389/fnins.2018.00500.
[27] P.T. Doughty, I. Hossain, C. Gong, K.A. Ponder, S. Pati, P.U. Arumugam, T. A. Murray, Novel microwire-based biosensor probe for simultaneous real-time measurement of glutamate and GABA dynamics in vitro and in vivo, Sci. Rep. 10 (2020), 12777, https://doi.org/10.1038/s41598-020-69636-1.
[28] S.S. Singh, P. Pal, A.K. Pandey, Y. Xing, K. Sato, Determination of precise crystallographic directions for mask alignment in wet bulk micromachining for MEMS, Micro Nano Syst. Lett. 4 (5) (2016), https://doi.org/10.1186/s40486-016-0027-5.
[29] C. Tan, P.T. Doughty, K. Magee, T.A. Murray, S. Siddiqui, P.U. Arumugam, Effect of process parameters on electrochemical performance of a glutamate microbiosensor, J. Electrochem. Soc. 167 (2020), 027528, https://doi.org/10.1149/1945-7111/ab6b0b.
[30] F. Pervin, W.W. Chen, Mechanically similar gel simulants for brain tissues, in: Proceedings of the SEM Annual Conference, Indianapolis, Indiana USA, ©2010 Society for Experimental Mechanics Inc, 2010, pp. 7–10. June.
[31] R. Pomfret, G. Miranpuri, K. Sillay, The substitute brain and the potential of the gel model, Ann. Neurosci. Psychol. 20 (2013), https://doi.org/10.5214/ans.0972.7531.200309, p. 118.
[32] M. Wang, L. Wang, X. Ji, Y. Bai, T. Li, S. ong, L. Li, Application of impedance spectroscopy for monitoring colloid Au-enhanced antibody immobilization and antibody-antigen reactions, Biosens. Bioelectron. 19 (2004) 575–582, https://doi.org/10.1016/s0956-5663(03)00252-5.
[33] T.G. Strein, A.G. Ewing, Characterization of small noble metal microelectrodes by voltammetry and energy-dispersive x-ray analysis, Anal. Chem. 65 (9) (1993) 1203–1209, https://doi.org/10.1021/ac00057a017.
[34] M.B. Alan, K.B. Oldham, C.G. Zoski, Steady state voltammetry, Anal. Chirnica Acta 216 (1989) 777 –-230.
[35] G. Dutta, S. Siddiqui, H. Zeng, J.A. Carlisle, P.U. Arumugam, The effect of electrode size and surface heterogeneity on electrochemical properties of ultrananocr ystalline diamond microelectrode, J. Electroanal. Chem. 756 (2015) 61–68, https://doi.org/10.1016/j.jelechem.2015.08.016.
[36] M.C. Steil, F. Thevenot, M. Kleitz, Densification of yttria - stabilized zirconia: impedance spectroscopy analysis, J. Electrochem. Soc. (1997), https://doi.org/10.1149/1.1837416/pdf.
[37] A. Amirudin, D. Thieny, Application of electrochemical impedance spectroscopy to study the degradation of polymer-coated metals, Prog. Org. Coat. 26 (1995) 1–28, https://doi.org/10.1016/0300-9440(95)00581-1.
[38] D.Z. De Florio, R. Muccillo, Sintering of zirconia-yttria ceramics studied by impedance spectroscopy, Solid State Ion. 123 (1999) 301–305, https://doi.org/10.1016/S0167-2738(99)00093-4.
[39] I.S. Beloborodov, P. Zapol, D.M. Gruen, L.A. Curtiss, Transport properties of n-type ultrananocrystalline diamond films, Phys. Rev. B - Condens. Matter Mater. Phys. 74 (2006) 1–5, https://doi.org/10.1103/PhysRevB.74.235434.
[40] T.Y. Pajkossy, Impedance of rough capacitive electrodes, J. Electroanal. Chem. 364 (1994) 111–125, https://doi.org/10.1016/0022-0728(93)02949-I.
[41] A. Weltin, J. Kieninger, B. Enderle, A.K. Gellner, B. Fritsch, G.A. Urban, Polymer-based, flexible glutamate and lactate microsensors for in vivo applications, Biosens. Bioelectron. 61 (2014) 192–199, https://doi.org/10.1016/j.bios.2014.05.014.
[42] E.M. Miller, J.E. Quintero, F. Pomerleau, P. Huettl, G.A. Gerhardt, P.E.A. Glaser, Simultaneous glutamate recordings in the frontal cortex network with multisite biomorphic microelectrodes: new tools for ADHD research, J. Neurosci. Methods 252 (2015) 75–79, https://doi.org/10.1016/j.jneumeth.2015.01.018.

Nicolaie Moldovan (Ph.D. in Physics) Founder of Alcorix Co and micro-nanofabrication expert with 25+ years of experience in materials, process, and device integration. His research interest is in micro-optics, MEMS and material sciences.

Iuliu-Ioan Blaga (MS Physics) Senior Researcher with Alcorix, with expertise in microfabrication, MEMS, microfluidics, as well as strong instrumentation skills from positions held at leading biotechnology companies. He developed microfluidic devices for proteomics and DNA sequencing, leading to publications in high-ranked journals and several patents.

Sanjeev Billa He is currently a Ph.D. student at Louisiana Tech University, Ruston, Louisiana. His research is to investigate advanced materials for multiplexed brain chemical sensing.

Imran Hossain (Ph.D. Micro/nano systems engineering) His research interests are on investigating new sensor fabrication and detection methods development for simultaneous detection of multiple neurotransmitters.

Chenggong Gong He is currently a Ph.D. student at Louisiana Tech. His research is to develop novel microscale electrodes and sensor packaging for *in vivo* tissue and animal models.

Claire E. Jones She is currently a Ph.D. student at Louisiana Tech. Her research is to identify mechanisms of brain injuries and neurological disorders.

Teresa A. Murray (Ph.D. Biomedical Engineering) She is an Associate Professor in Biomedical Engineering at Louisiana Tech. Her research focuses on identifying mechanisms of and evaluating therapies for brain injuries and neurological disorders.

Ralu Divan (Ph.D. Chemistry) Senior Chemist with the Center for Nanoscale Materials of Argonne National Laboratory. She has a 30+ years expertise in micro- and nanofabrication, materials, processes, and device integration. Her scientific interests rely in high resolution, high aspect ratio lithographic, etching, and growth processes for advanced micro- and nano-devices

Shabnam Siddiqui (Ph.D. Physics) She is an Assistant Professor in Department of Chemistry and Physics at Louisiana State University Shreveport, Louisiana. Her research focuses on understanding the electrochemical properties of nanomaterials and their application in chemical and biological sensing and energy storage.

Prabhu Arumugam (Ph.D. Microelectronics and Photonics) He is an Associate Professor in Mechanical Engineering and Institute for Micromanufacturing at Louisiana Tech. His research focuses on developing next generation electrochemical microsensor technologies with novel electrode geometries, nanomaterials, and new sensor detection strategies.